Extended detailed balance modeling toward solar cells with cement-based radiative coolers

Received: 30 June 2023 | Revised: 8 November 2023 | Accepted: 9 November 2023

DOI: 10.1002/pip.3758

SPECIAL ISSUE ARTICLE

PROGRESS IN PHOTOVOLTAICS WILEY

Extended detailed balance modeling toward solar cells with cement-based radiative coolers

Matteo Cagnoni[1] | Pietro Testa[1] | Jorge S. Dolado[2,3] | Federica Cappelluti[1]

[1]Department of Electronics and Telecommunications, Politecnico di Torino, Turin, Italy

[2]Centro de Física de Materiales, CSIC-UPV/EHU, San Sebastián, Spain

[3]Donostia International Physics Center, San Sebastián, Spain

Correspondence
Matteo Cagnoni, Department of Electronics and Telecommunications, Politecnico di Torino, Corso Duca degli Abruzzi 24, 10129 Turin, Italy.
Email: matteo.cagnoni@polito.it

Funding information
This research was supported by the European Union's Horizon 2020 Research and Innovation Program under grant agreement no. 964450.

Abstract

Reducing the temperature of a solar cell increases its efficiency and lifetime. This can be achieved by radiative cooling, a passive and simple method relying on materials that dump heat into outer space by thermal emission within the atmosphere transparency window between 8 and 13μm. As most radiative coolers are expensive or possibly UV unstable, we have recently proposed cement-based solutions as a robust and cost-effective alternative. However, the assessment model used describes the cell in the radiative limit and with perfect thermal coupling to the cooler, in line with the literature. In this work, we lift these two approximations, by incorporating Auger and Shockley–Read–Hall nonradiative recombination and a finite heat transfer coefficient at the cell/cooler interface, to obtain a thermal description of the cell/cooler stack closer to reality, while preserving the universality and transparency of the detailed-balance approach. We use this model to demonstrate that the cell performance gains provided by a radiative cooler are underestimated in the radiative limit and are hence more prominent in devices with stronger nonradiative recombination. Furthermore, we quantify the relation between cell temperature and heat transfer coefficient at the cell/cooler interface and show how this can be used to define design requirements. The extended model developed, and the resulting observations provide important guidelines toward the practical realization of novel radiative coolers for solar cells, including cement-based ones.

KEYWORDS
cementitious materials, detailed-balance principle, radiative cooling, solar cells

1 | INTRODUCTION

Following the experimental demonstration of subambient temperature under direct sunlight in 2014,[1] radiative cooling has been attracting a lot of interest in the scientific community as a thermal management solution for buildings and solar cells.[2] In solar cells, the strategy is to employ a radiative cooler as a heat sink that captures and radiates out of the system excess heat generated upon sunlight absorption,[3] as shown in Figure 1. The resulting temperature reduction brings two important benefits to the solar cell: (1) it enhances its power conversion efficiency, by roughly 0.45%/K of relative increase in silicon-based devices[4] and (2) it extends its lifetime, by about $2\times/10\text{K}$ according to an estimate based on Arrhenius' law.[5]

The defining feature of radiative coolers is their ability to emit as much thermal radiation as a black-body (BB) within the so-called atmosphere transparency window (AW) between 8 and 13μm, quantified by a spectral emissivity A_λ^{RC} close to unity.[7] Because the BB radiation is peaked inside the AW at terrestrial temperatures, these bodies

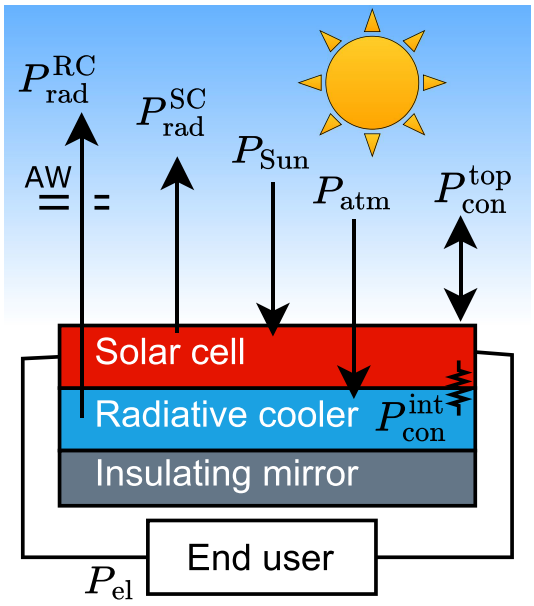

FIGURE 1 Working principle of a photovoltaic system with radiative cooler. The energy exchange terms between solar cell, radiative cooler, environment, and end user are depicted, together with the possible thermal resistance at the interface between cell and cooler. These do not exchange energy by radiation because they operate in separate ranges of the electromagnetic spectrum, namely, UV-visible and IR, respectively. Here, the cooler is depicted below because this geometry is expected to be more feasible with cement-based materials, in particular in the context of building-integrated photovoltaic systems. For simplicity, a mirror with ideal reflection and thermal insulation properties is placed at the bottom of the device. [Colour figure can be viewed at wileyonlinelibrary.com]

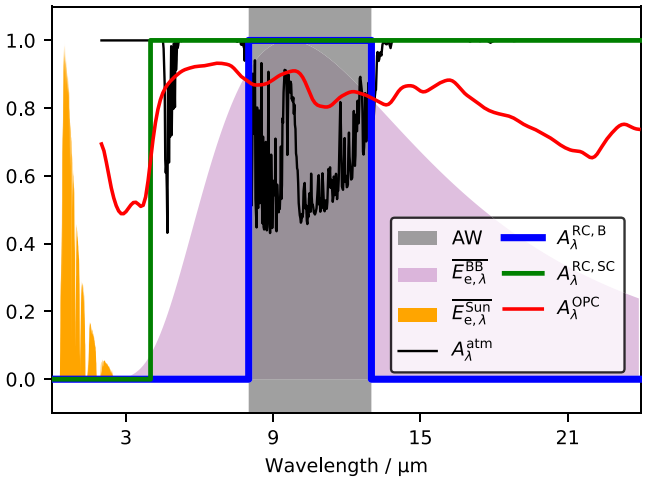

FIGURE 2 Comparison between atmospheric window (AW), normalized spectral irradiance of a black-body (BB) at ambient temperature ($\overline{E_{e,\lambda}^{BB}}$) and of the Sun ($\overline{E_{e,\lambda}^{Sun}}$), and spectral emissivity of the atmosphere (A_λ^{atm}), of the ideal radiative cooler for buildings ($A_\lambda^{RC,B}$) and solar cells ($A_\lambda^{RC,SC}$), and of the radiative cooler made of Ordinary Portland Cement (OPC) paste (A_λ^{OPC}) considered in this study and taken from.[6] [Colour figure can be viewed at wileyonlinelibrary.com]

eject a large amount of heat as electromagnetic waves at these wavelengths. This energy outflow is not compensated for by re-absorption within the AW, despite Kirchhoff's law on the equivalence between emissivity and absorbance spectra.[8] Indeed, the main radiation sources, that is, the Sun and the atmosphere, are inactive and weakened, respectively, in this spectral range. On the other hand, the atmosphere emits a significant amount of thermal radiation outside of the AW. At these wavelengths, compensation of the thermal energy radiated within the AW may occur, depending on whether or not the cooler has the potential to reach a subambient temperature in the system and environment considered. If this is the case, as in buildings, the cooler emissivity must be suppressed outside of the AW, to prevent a net incoming energy flux that would nuance the temperature reduction (selective emitter). On the contrary, if subambient temperatures are not reachable, for example, because of additional heat from a solar cell that keeps the cooler temperature above ambient, the cooler emissivity must be maximized also outside of the AW, to take advantage of an additional net outgoing energy flux (broad-band emitter). These considerations lead to the definition of a different ideal emissivity spectrum for radiative coolers applied to buildings ($A_\lambda^{RC,B}$) and solar cells ($A_\lambda^{RC,SC}$), as shown in Figure 2, where also the other spectra invoked above are depicted.[9]

Attracted by the passive nature, expected efficiency, and systemic simplicity of this thermal management solution, researchers have developed several kinds of radiative coolers,[10,11] such as stratified[1,12,13] or surface-patterned[3,14,15] meta-materials and hierarchical porous polymers.[16,17] Because of the reliance of the former on scarce elements (Ag, Hf)[18] or complex fabrication processes and the potential UV instability of the latter,[9] large-scale applicability of these solutions is unclear.

In an attempt to combine performance, low cost and reliability, we have recently proposed cement-based materials as a novel class of radiative coolers for solar cells.[6,19] In these works, we have predicted that the spectral emissivity of a 100μm slab of Ordinary Portland Cement (OPC) paste[20] with a properly engineered microstructure could approach the spectrum of the ideal broad-band emitter for solar cells, as shown in Figure 2. These predictions agree with recent experimental work on similar materials[21,22] and could imply a temperature reduction in silicon-based solar cells of up to 19K according to the principle of detailed balance, leading to up to 9 % of efficiency relative increase and up to four times of lifetime extension.

Yet, our theoretical assessment has relied on the state-of-the-art detailed-balance model commonly employed to describe the energetics of photovoltaic systems with radiative coolers,[3,15,23] which makes two important assumptions: (1) the solar cell is described by the Shockley–Queisser (SQ) model in the radiative limit,[24] that is, radiative (RAD) recombination of photo-generated charge carriers is the only electrical loss mechanism taken into account; (2) the cell and the cooler are assumed to have perfect thermal coupling, that is, they are isothermal.

In this work, we have extended our previous analysis by lifting these two approximations, to obtain a more accurate evaluation of the cooling potential of the cement paste considered and useful guidelines at material/device level. In particular:

1. We have started by incorporating Auger (AUG) and Shockley–Read–Hall (SRH) nonradiative recombination[25] into the SQ model that describes the solar cell within the system depicted in Figure 1;

their dependence on temperature suggests a significant impact on the thermal behavior of the system. To the best of our knowledge, in the context of detailed-balance descriptions of photovoltaic systems with radiative coolers, Auger recombination has been considered only once,[26] though only for the specific case of silicon-based devices, while SRH recombination has never been. To discuss their impact in a general setting and refrain from limiting ourselves to specific cases, we have incorporated these mechanisms in a parametric form that separates their dependence on temperature from the one on quantities characteristic of a given material/technology. The latter are grouped into a pair of values per mechanism, namely, the semiconductor band gap E_g and a hereby defined β parameter quantifying the strength of the nonradiative recombination channel considered (β_{AUG} for Auger, β_{SRH} for SRH). This has let us express the temperature reduction and associated efficiency gain brought by the radiative cooler as a function of the triplet $(E_g,\beta_{AUG},\beta_{SRH})$ only, which encapsulates the most relevant properties of a given solar cell material/technology and simplifies the treatment by merging quantities with indistinguishable impact on the device performance into a single one.

2. Then, we have lifted the approximation of perfect thermal coupling between cell and cooler by introducing a finite heat transfer coefficient h_c^{int} at their interface,[27] as shown in Figure 1. The corresponding thermal resistance cannot be neglected, because of the poor adhesion properties of cement-based materials,[28] and might play a role also in solutions with better mechanical properties but affected by acoustic mismatch.[29] The resulting thermal barrier establishes a temperature difference between cell and cooler, weakening the cell temperature reduction. We have quantified this effect and defined thermal contact requirements for the cement-based radiative cooler.

2 | METHODS

To assess the radiative cooling performance, we have compared the solar cell operating temperature with and without a thermally coupled cement slab having the spectral emissivity of Figure 2. We have determined this temperature by considering the detailed-balance model depicted in Figure 1, describing the energetics of the device and its environment. For simplicity, a mirror with ideal reflection and thermal insulation is placed at the bottom of the device, so that all energy exchanges between the latter and the environment take place on the same top surface. We have adopted a configuration with the cooler below the cell to prevent blocking of the solar radiation by the former and make the design feasible also for bulky materials such as cements, with a eye toward building-integrated photovoltaics[30]; solar cells built onto building structural elements have been reported in the recent literature.[31–33] To not block the radiation emitted by the cooler, the cell must have enough contact-free space, with bifacial devices[34] being more attractive in this sense, and a cover glass transparent around the atmospheric window, such as a polyethylene-based one.[35] Alternatively, one could envision the use of a radiative cooler with fast planar heat propagation and part or all of its surface area free from the solar cell,[36] from which to eject thermal radiation.

Thanks to this model, one can obtain the net power density of the cell (P_{net}^{SC}) and the cooler (P_{net}^{RC}) as a function of their temperatures T_{SC} and T_{RC} and of other quantities dependent on the technology considered and on the environmental conditions, according to the following equations:

$$P_{net}^{SC} = \underbrace{P_{rad}^{SC} - P_{Sun}}_{\text{UV-visible}} + P_{el} + P_{con}^{top} + P_{con}^{int} \tag{1a}$$

$$P_{net}^{RC} = \underbrace{P_{rad}^{RC} - P_{atm}}_{\text{IR}} - P_{con}^{int} \tag{1b}$$

P_{rad}^{SC}, P_{Sun}, P_{el}, and P_{con}^{top} are the power density that the cell radiates in the UV-visible, absorbs from the Sun, delivers to the end user as electricity, and exchanges with the environment by conduction/convection at its top surface, respectively. On the other hand, P_{rad}^{RC} and P_{atm} are the power densities that the cooler radiates in the IR and absorbs from the atmosphere, respectively, while its conductive/convective heat exchange with the environment is suppressed by the perfect thermal insulator at its bottom surface. Finally, the cell and the cooler exchange heat by conduction at their interface, with a corresponding power density P_{con}^{int}. This term is the sole responsible for their thermal coupling, since they operate in separate ranges of the electromagnetic spectrum, namely, the UV-visible and the IR, and hence are mutually transparent, as can be inferred from the spectra reported in Figure 2. This electromagnetic decoupling renders the stacking order of cell and cooler unimportant from the detailed-balance perspective, making the conclusions of this work valid also for the inverted configuration as long as the cooler is transparent at solar wavelengths.

The working point of the system corresponds to its steady state, in which the net power density is zero everywhere.[27] Accordingly, we have determined the operating temperature of cell and cooler by solving the system of equations below, where only the independent variables to be determined, that is, T_{SC} and T_{RC}, have been written explicitly for the sake of clarity:

$$\begin{cases} P_{net}^{SC}(T_{SC},T_{RC}) = 0 \\ P_{net}^{RC}(T_{SC},T_{RC}) = 0 \end{cases} \tag{2}$$

If perfect thermal coupling between cell and cooler is assumed, then these are isothermal, that is, $T_{SC} = T_{RC} = T$, and Equation (2) reduces to $P_{net}(T) = 0$, with

$$P_{net} = P_{rad}^{SC} - P_{Sun} + P_{el} + P_{rad}^{RC} - P_{atm} + P_{con}^{top} \tag{3}$$

This isothermal model is the one typically employed in the literature[15,23,26]; by generalizing it to the case of nonzero thermal contact resistance, that is, finite heat transfer coefficient, at the cell/cooler interface (Equations 1a, 1b, and 2), we have enabled the description of a larger set of systems.

As discussed in Section 1, we have first incorporated Auger and SRH recombination into the computation of P_{el} by adopting the following expression for the cell current density J as a function of its voltage V:

$$J(V) = \underbrace{J_{PHT} - J_{RAD}(V)}_{\text{radiative limit}} - J_{AUG}(V) - J_{SRH}(V) \tag{4}$$

where only the independent variable V has been written explicitly for the sake of clarity. Then, we have calculated P_{el} as the product between the cell output current density and voltage at maximum-power-point (MPP):

$$P_{el} = J_{MPP} V_{MPP} = \max_{V} \{J(V) V\} \tag{5}$$

In Equation (4), J_{PHT}, J_{RAD}, J_{AUG}, and J_{SRH} are the current densities corresponding to photo-generation and radiative, Auger, and SRH recombination of charge carriers, respectively. J_{PHT} and J_{RAD} are the only terms considered in the original SQ model,[24] corresponding to the radiative limit, that is, the case with negligible nonradiative recombination; we have calculated them by multiplying the photon absorption and emission rates for the elementary charge e. At the same time, we have used well-established expressions for the Auger[37] and SRH[38] current densities. The corresponding equations, with all dependencies explicitly written, are as follows:

$$J_{PHT}(E_g) = e \int_0^{hc/E_g} d\lambda \frac{\lambda}{hc} E_{e,\lambda}^{Sun}(\lambda) \tag{6a}$$

$$J_{RAD}(T, V, E_g) = e\pi \int_0^{hc/E_g} d\lambda \frac{\lambda}{hc} L_{e,\Omega,\lambda}^{BB}(\lambda, T, V) \tag{6b}$$

$$J_{AUG}(T, V, E_g, \beta_{AUG}) = J_{AUG}^{(0)}(T, E_g, \beta_{AUG}) \exp\left(\frac{3eV}{2kT}\right) \tag{6c}$$

$$J_{SRH}(T, V, E_g, \beta_{SRH}) = J_{SRH}^{(0)}(T, E_g, \beta_{SRH}) \exp\left(\frac{eV}{2kT}\right) \tag{6d}$$

Here, $E_{e,\lambda}^{Sun}$ is the AM1.5g Sun spectral irradiance[39]; $L_{e,\Omega,\lambda}^{BB} = \frac{2hc^2}{\lambda^5}\left[\exp\left(\frac{hc/\lambda - eV}{kT}\right) - 1\right]^{-1}$ is the BB spectral radiance under bias[40]; T, V, and E_g are the solar cell temperature, output voltage, and band gap, respectively; λ is the radiation wavelength; and c, h, and k are speed of light, Planck's constant, and Boltzmann's constant.

We have already adopted the hereby defined β parameters in Equations (6c) and (6d), whose motivation has been given in the Introduction:

$$\beta_{AUG} = eWC_{AUG}(300K) N_v^{3/2}(300K) N_c^{3/2}(300K) \tag{7a}$$

$$\beta_{SRH} = \frac{eWN_v^{1/2}(300K) N_c^{1/2}(300K)}{2\tau_{SRH}(300K)} \tag{7b}$$

Here, C_{AUG}, τ_{SRH}, N_v, N_c, and W are the Auger coefficient, SRH lifetime, valence and conduction band effective density-of-states, and thickness of the solar cell semiconductor. The β parameters quantify the strength of the corresponding nonradiative recombination mechanism and have let us separate temperature dependence from technology-dependent quantities. Their definition naturally emerges from the expressions[37,38]

$$J_{AUG}^{(0)} = eWC_{AUG} n_i^3 = \beta_{AUG} \left(\frac{T}{300K}\right)^5 \exp\left(-\frac{3E_g}{2kT}\right) \tag{8a}$$

$$J_{SRH}^{(0)} = \frac{eWn_i}{2\tau_{SRH}} = \beta_{SRH} \left(\frac{T}{300K}\right)^3 \exp\left(-\frac{E_g}{2kT}\right) \tag{8b}$$

where n_i is the semiconductor intrinsic carrier concentration, upon application of the following substitutions[41,42]:

$$C_{AUG} = C_{AUG}(300K) \left(\frac{T}{300K}\right)^{1/2} \tag{9a}$$

$$\tau_{SRH} = \tau_{SRH}(300K) \left(\frac{T}{300K}\right)^{-3/2} \tag{9b}$$

$$n_i = \sqrt{N_c N_v} \exp\left(-\frac{E_g}{2kT}\right) \tag{9c}$$

$$N_v = N_v(300K) \left(\frac{T}{300K}\right)^{3/2} \tag{9d}$$

$$N_c = N_c(300K) \left(\frac{T}{300K}\right)^{3/2} \tag{9e}$$

Several expressions are available in the literature for the temperature dependence of the Auger coefficient[43–45]; for completeness, we have verified that they provide results comparable with Equation (9a).

We have calculated the other power densities appearing in Equation (3) as follows[6]:

$$P_{rad}^{SC} = \pi \int_0^{hc/E_g} d\lambda L_{e,\Omega,\lambda}^{BB}(\lambda, T_{SC}, V_{MPP}) \tag{10a}$$

$$P_{Sun} = \int_0^{hc/E_g} d\lambda E_{e,\lambda}^{Sun}(\lambda) \tag{10b}$$

$$P_{rad}^{RC} = \int_0^{2\pi} d\Omega \cos\theta \int_0^{+\infty} d\lambda A_{\Omega,\lambda}^{RC}(\lambda, \theta) L_{e,\Omega,\lambda}^{BB}(\lambda, T_{RC}, 0) \tag{10c}$$

$$P_{atm} = \int_0^{2\pi} d\Omega \cos\theta \int_0^{+\infty} d\lambda A_{\Omega,\lambda}^{atm}(\lambda, \theta) A_{\Omega,\lambda}^{RC}(\lambda, \theta) L_{e,\Omega,\lambda}^{BB}(\lambda, T_0, 0) \tag{10d}$$

$$P_{con}^{top} = h_c^{top}(T_{SC} - T_0) \tag{10e}$$

where $T_{SC} = T_{RC} = T$ in case of perfect cell/cooler thermal contact. Here, $A_{\Omega,\lambda}^{RC}$ is the spectral directional absorbance/emissivity of the

radiative cooler (equal to the one of the cement paste considered from Cagnoni et al.,[6] $A^{OPC}_{\Omega,\lambda}$, whose associated spectral absorbance/emissivity is shown in Figure 2), $A^{atm}_{\Omega,\lambda}$ is the one of the atmosphere, for which we have taken the summer spectrum included in RadCool[46] from MODTRAN,[47] $h^{top}_c = 10.6\,\mathrm{W m^{-2} K^{-1}}$ is the heat transfer coefficient between cell and environment (set to this value to reproduce the case of average winds[26]), $T_0 = 293.15\,\mathrm{K}$ is the atmosphere (ambient) temperature, and θ is the zenith angle of a spherical coordinate system with origin on the solar cell top surface and associated z-axis normal to such a surface.

Finally, we have modeled the nonzero thermal resistance at the cell/cooler interface entering the nonisothermal model with the following linear relation[27]:

$$P^{int}_{con} = h^{int}_c (T_{SC} - T_{RC}) \tag{11}$$

where h^{int}_c is an empirical heat transfer coefficient.

We refer the reader to the literature for more details concerning the definition of the radiometry quantities employed.[8]

3 | RESULTS

We have started by simulating the temperature dependence of the power conversion efficiency at MPP $\eta = P_{el}/P^{tot}_{Sun}$ of two of the most representative single-junction solar cell technologies, namely, silicon (Si) and gallium arsenide (GaAs), without cooler. $P^{tot}_{Sun} \approx 1000\,\mathrm{W m^{-2}}$ is the total power density incoming from the Sun, which can be obtained by integrating $E^{Sun}_{e,\lambda}$ across all wavelengths. On the other hand, we have obtained P_{el} by plugging Equation (4) into Equation (5). In particular, we have considered the radiative limit ($J_{AUG} = 0$ and $J_{SRH} = 0$) and the cases where Auger and SRH recombination are individually or simultaneously accounted for by setting $J_{AUG} \neq 0$ and/or $J_{SRH} \neq 0$. The results of the simulations are shown in Figure 3A for silicon and Figure 3B for gallium arsenide, while the model parameters used are summarized in Table 1 together with their sources.

First, the predicted power conversion efficiency becomes smaller for all temperatures as more recombination channels are taken into account. In addition to this fairly trivial result, the calculated curves show that the predicted temperature coefficient of the power conversion efficiency $\partial_T \eta$ increases by approximately a factor of 2 as more nonradiative mechanisms are included. Since this corresponds to a better description of the device behavior, it implies that the temperature-driven performance degradation of single-junction solar cells is underestimated in the radiative limit. Moreover, since the lower power conversion efficiency implies that less energy is delivered to the end user, additional energy remains trapped within the cell, with a resulting heating effect that cannot be compensated for by

TABLE 1 Parameter values used for the simulation of Si and GaAs solar cells, namely, band gap E_g, thickness W, Auger coefficient C_{AUG}, SRH lifetime τ_{SRH}, and valence and conduction band effective density-of-states N_v and N_c of the solar cell semiconductor.

	Si	GaAs
E_g / eV	1.12[41]	1.43[41]
W / μm	200[25]	2[48]
$C_{AUG}(300\mathrm{K})$ / $\mathrm{cm^6 s^{-1}}$	3.88×10^{-31}[45]	1.00×10^{-30}[41]
$\tau_{SRH}(300\mathrm{K})$ / s	10×10^{-3}[49]	1×10^{-6}[50]
$N_c(300\mathrm{K})$ / $\mathrm{cm^{-3}}$	3.22×10^{19}[41]	4.45×10^{17}[51]
$N_v(300\mathrm{K})$ / $\mathrm{cm^{-3}}$	1.80×10^{19}[41]	7.72×10^{18}[51]

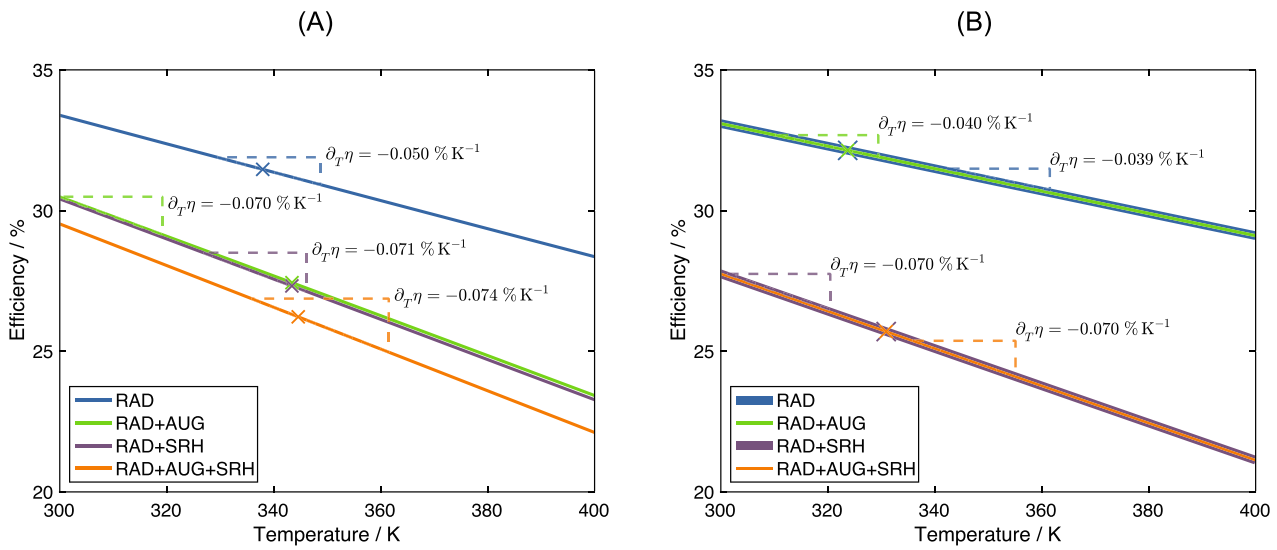

FIGURE 3 Temperature dependence of the power conversion efficiency of single-junction solar cells calculated with a Shockley–Queisser model incorporating different combinations of radiative and nonradiative losses of photo-generated charge carriers: (A) silicon (Si) based solar cell. (B) Gallium arsenide (GaAs)-based solar cell. (C) The temperature coefficient $\partial_T \eta$ of the lines is reported together with the solar cell operating (steady-state) temperature, which is marked by a cross. [Colour figure can be viewed at wileyonlinelibrary.com]

the corresponding slight increase of thermal emission due to radiative recombination. This suggests that the solar cell settles at a higher operating temperature than the one predicted in the radiative limit, as we have confirmed by determining the solar cell steady-state temperature for all recombination settings considered in Figure 3A,B. In particular, we have solved $P_{\text{net}}^{\text{SC}} = 0$ with respect to T_{SC} for the case without radiative cooler, which can be obtained by setting $P_{\text{con}}^{\text{int}} = 0$ in Equation (1a). The obtained (T_{SC}, η) working points are marked by a cross in Figure 3A,B, and, as expected, move toward higher temperatures as more nonradiative recombination channels are taken into account. In conclusion, by incorporating nonradiative terms into the detailed-balance description of the solar cell, we have verified that the solar cell efficiency is lower than what is expected in the radiative limit not only because of the higher overall recombination rate at fixed temperature but also because the presence of nonradiative recombination leads to a higher operating temperature, whose corresponding performance degradation is amplified by the larger temperature coefficient $\partial_T \eta$.

Next, we have determined the cell temperature reduction $\Delta T_{\text{SC}} = T_{\text{SC}}(\text{with cooler}) - T_{\text{SC}}(\text{without cooler})$ and power conversion efficiency gain $\Delta\eta = \eta(\text{with cooler}) - \eta(\text{without cooler})$ as a function of the solar cell band gap E_{g} and nonradiative recombination strength β, for both Auger (β_{AUG}) and SRH (β_{SRH}) mechanisms, in the case of perfect coupling to the cement-based radiative cooler considered. By parametrically varying E_{g}, β_{AUG}, and β_{SRH}, we have covered all the systems that can be described by the detailed-balance model used in this work. Analysis of a certain solar cell material/technology can be done by simply identifying the corresponding $(E_{\text{g}}, \beta_{\text{AUG}}, \beta_{\text{SRH}})$ point.

The results of our simulations are shown in Figures 4 and 5, where we have considered the model with radiative and Auger recombination, but no SRH ($\beta_{\text{AUG}} \neq 0$ and $\beta_{\text{SRH}} = 0$), and the model with radiative and SRH recombination, but no Auger ($\beta_{\text{SRH}} \neq 0$ and $\beta_{\text{AUG}} = 0$), respectively. Thanks to this separation, we have obtained 2D maps that provide a clear and convenient graphical representation of the interplay between solar cell band gap, strength of the nonradiative recombination channels, and performance of the radiative cooler.

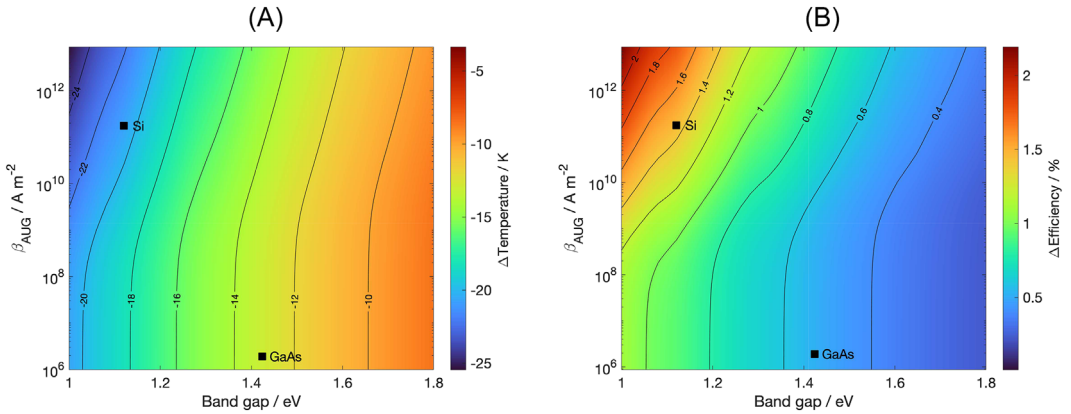

FIGURE 4 Performance of the cement-based radiative cooler as a function of the solar cell band gap and Auger recombination strength, with radiative recombination accounted for, but SRH recombination neglected: (A) solar cell operating temperature variation. (B) Solar cell power conversion efficiency gain. [Colour figure can be viewed at wileyonlinelibrary.com]

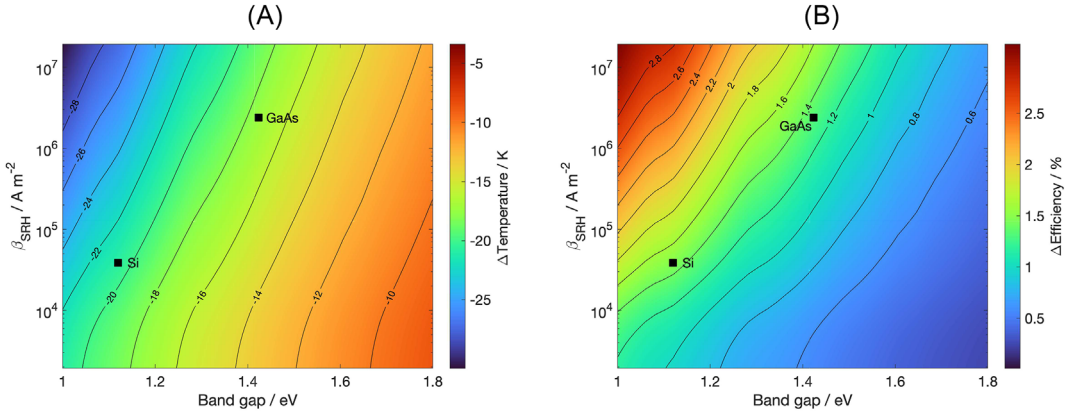

FIGURE 5 Performance of the cement-based radiative cooler as a function of the solar cell band gap and Shockley–Read–Hall (SRH) recombination strength, with radiative recombination accounted for, but Auger recombination neglected: (A) solar cell operating temperature variation. B) solar cell power conversion efficiency gain. [Colour figure can be viewed at wileyonlinelibrary.com]

For completeness, we have highlighted the points corresponding to silicon and gallium arsenide solar cells, by assigning the values corresponding to Table 1 to E_g, β_{AUG}, and β_{SRH}.

The impact of the radiative cooler is more significant for larger values of the β parameters, that is, for increasing strength of Auger and SRH recombination, regardless of the solar cell band gap. This can be readily inferred from Figures 4A and 5A, by observing that increasing β corresponds to crossing "equipotential" curves with increasing ΔT_{SC}. This behavior is due to the tendency of the cell and thus the cooler to reach a higher temperature, which increases the amount of thermal radiation emitted and the subsequent reduction in temperature. As consequence, the benefits of radiative cooling are more prominent in devices departing from the radiative limit (intercept with the E_g axis), which leads to an underestimation of the obtainable gains, although the cooling performance is excellent also in cells with negligible nonradiative recombination. Indeed, below a certain β, the temperature reduction becomes independent of this parameter ("vertical" equipotential curves) at a ΔT_{SC} large enough to make radiative cooling worth pursuing. As a matter of fact, the major player in rendering radiative cooling ineffective is the band gap, with the induced temperature reduction decreasing by more than a factor of 2 from 1.0 to 1.8eV because of the the lower cell operating temperature, which is caused by the reduced thermalization of charge carriers. Finally, since both temperature reduction and temperature coefficient of the power conversion efficiency increase with increasing β parameters, also the efficiency gain provided by the radiative cooler becomes more prominent, as can be seen on the maps in Figures 4B and 5B.

According to this extended model, our cement-based radiative cooler is expected to provide a temperature reduction of ~21 K and a corresponding absolute efficiency gain of ~ 1.4 %, instead of the ~19 K, and ~ 0.7 % predicted by the radiative limit, the former efficiency value being closer to the well-established thumb rule reported in the literature[4] that suggests a 0.45%/K of efficiency relative increase; a better match could probably be achieved by considering also the temperature dependence of the solar cell internal quantum efficiency, which is though well beyond the purpose of the present work. At the same time, according to considerations on chemical reaction rates based on Arrhenius' law,[5] this temperature reduction could extend the solar cell lifetime by a factor of four. In conclusion, the gains brought by the application of a cement-based radiative cooler to a solar cell are expected to be even better than what has been predicted in our previous analysis performed in the radiative limit.[6] Given the low cost, availability and scalability of cement-based materials, the benefits-to-cost ratio is expected to be high, rendering the experimental realization of this concept extremely attractive.

At last, we have investigated the impact of the thermal contact resistance at the cell/cooler interface, which takes a decidedly important role in our proposed class of radiative coolers because of the poor adhesion properties of cement-based materials.[28] To minimize the number of parameters affecting the results and preserve their universality and easy visualization, we have performed this step in the radiative limit, aware that the qualitative conclusions reached are not going to be invalidated by considering also nonradiative recombination channels. We have determined the solar cell and radiative cooler

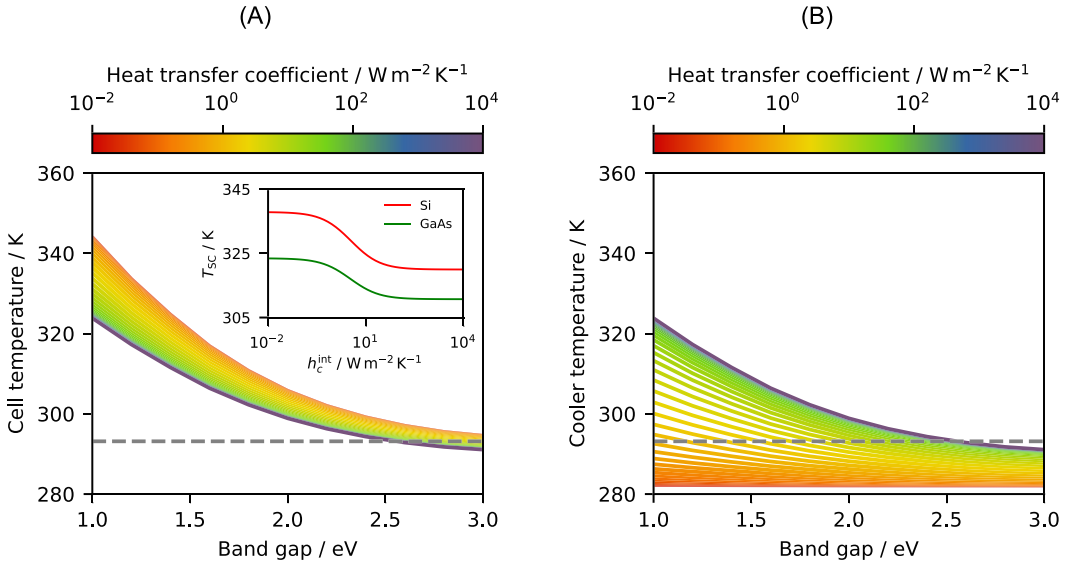

FIGURE 6 Impact of the thermal resistance at the cell/cooler interface for different values of the heat transfer coefficient: (A) Solar cell temperature as a function of the band gap for several values of the heat transfer coefficient; the inset shows the operating temperature of silicon and gallium arsenide solar cells as a function of the heat transfer coefficient. (B) Radiative cooler temperature as a function of the band gap for several values of the heat transfer coefficient. Above a certain heat transfer coefficient, the approximation of perfect thermal coupling is legit, as the cell and the cooler almost have the same steady-state temperature. On the other hand, below a certain heat transfer coefficient, they become completely decoupled and behave as independent entities. The difference between the temperatures in these two extreme cases corresponds to maximum achievable solar cell temperature reduction. For values in between, the solar cell settles at a higher temperature, whose value depends on the heat transfer coefficient, as can be seen from the inset. Upon definition of system specifications that fix the highest acceptable solar cell temperature, one can define a minimum heat transfer coefficient as a design requirement. [Colour figure can be viewed at wileyonlinelibrary.com]

temperatures, which in this case become different from each other, by solving the system given in Equation (2) with respect to T_{SC} and T_{RC}, with P_{net}^{SC} and P_{net}^{RC} given by Equations (1a) and (1b), respectively. We have considered a wide range of values for the interface thermal contact resistance h_c^{int}, given our purpose to define design guidelines rather than characterize a specific device.

The results of our simulations are reported in Figure 6A,B, showing the steady-state temperature of the solar cell and the radiative cooler as a function of the solar cell band gap for several values of h_c^{int}. When $h_c^{int} > 10^2 \mathrm{W m^{-2} K}$ (approximately), heat transfer at the interface is very effective and the solar cell and the radiative cooler are able to follow each other's temperature, hence keeping the system into an isothermal steady-state; in this case, the approximation of perfect thermal coupling is legit. On the other hand, when $h_c^{int} < 10^{-1} \mathrm{W m^{-2} K^{-1}}$ (approximately), heat transfer at the interface is almost completely hindered and the cell and the cooler behave as two thermally independent bodies. Of course, this leads to a much higher solar cell temperature that degrades performance and lifetime. Finally, the steady-state temperature of the solar cell varies almost linearly with $\log_{10}\left(h_c^{int} \mathrm{W^{-1} m^2 K}\right)$ and a "logarithmic coefficient" quantifying the relation between T_{SC} and h_c^{int} for a given E_g can be defined; these observations are clearer in the inset of Figure 6A, where the solar cell operating temperature as a function of the interface heat transfer coefficient is shown for silicon and gallium arsenide devices. Depending on the needed solar cell temperature, this coefficient can be used to define requirements for the thermal resistance at the cell/cooler interface, whose achievement must be validated experimentally. These results can be readily extended to the case of nonnegligible nonradiative recombination mechanisms, by setting the β parameters to the values corresponding to the solar cell considered. In conclusion, the radiative cooler must be able to fulfill the observed thermal coupling requirements, by providing a heat transfer coefficient of at least $1 \mathrm{W m^{-2} K^{-1}}$ (approximately); depending on the minimum acceptable solar cell temperature reduction, larger values might be needed and can be identified from curves analogous to the inset in Figure 6A. The interface heat transfer coefficient of a real device could be characterized experimentally[52] on a planar sample consisting of the bottom solar cell material stacked onto a slab of the cement considered. If unsatisfactory, the adhesion properties could be tuned by taking advantage of the numerous chemical and micro-structural landscape of cement-based materials,[28] which enable a wide control of the material properties. This tunability makes us optimistic concerning the practical realization of photovoltaic systems with cement-based radiative coolers.

4 | CONCLUSIONS

In this work, we have first extended the detailed-balance model commonly employed in the literature to assess radiative coolers for solar cells, by incorporating Auger and SRH nonradiative recombination. Beside trivially reducing the overall power conversion efficiency, these mechanisms also increase the cell operating temperature and the reduction rate of its efficiency with increasing temperature.

Then, we have shown that the absolute temperature reduction and the corresponding power conversion efficiency gain become stronger when nonradiative recombination is prominent. Therefore, neglecting nonradiative recombination may lead to an underestimation of the benefits provided by a radiative cooler, with these benefits being slightly weakened, but far from negligible, in cells well-described by the radiative limit. By discussing the impact of these nonradiative recombination channels in a very general setting thanks to the introduction of the β terms, we have minimized the number of independent parameters and described the problem in very accessible terms, reaching conclusions independent of the specific solar cell implementation.

Next, we have demonstrated that a thermal contact resistance at the cell/cooler interface leads to their partial (or total) decoupling and identified the conditions for (approximately) perfect thermal coupling and isothermal system, complete thermal decoupling, and partial reduction of the cooling effect. We have also discussed how this model can be used to define thermal contact requirements from the specification of the temperature reduction needed to achieve the desired solar cell performance.

We have performed the extension of the detail-balance model with the intention of getting closer to the practical realization of solar cells with cement-based radiative coolers, a solution proposed in our recent work.[6] Taking nonradiative recombination into account has allowed us to model the solar cell more realistically and prove that the benefits provided by the introduction of the cement-based radiative cooler are even more significant than previously estimated. The finite heat transfer coefficient is going to weaken these benefits, but we have defined design guidelines that should enable device engineers to identify the minimum value of this parameter needed to obtain the desired cooling performance. Given the outstanding property tunability of cement-based materials,[28] we are optimistic concerning their capability to fulfill eventual thermal coupling requirements. The practical realization of this concept, for which we have provided some hints, is extremely attractive because of its remarkable gain-to-cost ratio and fits very well into the context of building-integrated photovoltaics. Worth noting, solar cells placed onto building structural elements have already been reported in the literature,[31–33] although with no discussion concerning radiative cooling.

The models developed and the conclusions reached can be easily transferred to other radiative coolers, by adapting the spectral directional emissivity that enters the detailed-balance equations, and are expected to provide important guidelines toward the practical realization of novel solutions.

AUTHOR CONTRIBUTIONS

Conceptualization: M.C., P.T., and F.C. Data curation: M.C. and P.T. Formal analysis: M.C. and P.T. Funding acquisition: J.D. and F.C. Investigation: M.C. and P.T. Methodology: M.C. and P.T. Project administration: J.D. and F.C. Resources: M.C. and P.T. Software: M.C. and P.T. Supervision: M.C. and F.C. Validation: M.C. and P.T.

Visualization: M.C. and P.T. Writing - original draft: M.C. Writing - review & editing: M.C., P.T., J.D., and F.C.

ACKNOWLEDGMENTS

This project has received funding from the European Union's Horizon 2020 Research and Innovation Program under grant agreement no. 964450.

CONFLICT OF INTEREST STATEMENT

The authors declare no potential conflict of interests.

DATA AVAILABILITY STATEMENT

The data that support the findings of this study are available from the corresponding author upon reasonable request.

ORCID

Matteo Cagnoni https://orcid.org/0000-0003-0599-1715
Pietro Testa https://orcid.org/0000-0003-3877-8427
Jorge S. Dolado https://orcid.org/0000-0003-3686-1438
Federica Cappelluti https://orcid.org/0000-0003-4485-9055

REFERENCES

1. Raman AP, Anoma MA, Zhu L, Rephaeli E, Fan S. Passive Radiative Cooling Below Ambient Air Temperature Under Direct Sunlight. *Nature*. 2014;515(7528):540-544. doi:10.1038/nature13883
2. Zeyghami M, Goswami DY, Stefanakos E. A Review of Clear Sky Radiative Cooling Developments and Applications in Renewable Power Systems and Passive Building Cooling. *Solar Energy Mater Solar Cells*. 2018;178:115-128. doi:10.1016/j.solmat.2018.01.015
3. Zhu L, Raman A, Wang KX, Anoma MA, Fan S. Radiative Cooling of Solar Cells. *Optica*. 2014;1(1):32. doi:10.1364/OPTICA.1.000032
4. Skoplaki E, Palyvos JA. On the Temperature Dependence of Photovoltaic Module Electrical Performance: A Review of Efficiency/Power Correlations. *Solar Energy*. 2009;83(5):614-624. doi:10.1016/j.solener.2008.10.008
5. Dupré O, Vaillon R, Green MA. *Thermal Behavior of Photovoltaic Devices: Physics and Engineering*: Springer; 2017.
6. Cagnoni M, Tibaldi A, Dolado JS, Cappelluti F. Cementitious Materials as Promising Radiative Coolers for Solar Cells. *iScience*. 2022;25(11):105320. doi:10.1016/j.isci.2022.105320
7. Catalanotti S, Cuomo V, Piro G, Ruggi D, Silvestrini V, Troise G. The Radiative Cooling of Selective Surfaces. *Solar Energy*. 1975;17(2):83-89. doi:10.1016/0038-092X(75)90062-6
8. Balaji C. *Essentials of Radiation Heat Transfer*: Ane Books; 2014.
9. Zhao D, Aili A, Zhai Y, et al. Radiative Sky Cooling: Fundamental Principles, Materials, and Applications. *Appl Phys Rev*. 2019;6(2):21306. doi:10.1063/1.5087281
10. Bijarniya JP, Sarkar J, Maiti P. Review on Passive Daytime Radiative Cooling: Fundamentals, Recent Researches, Challenges and Opportunities. *Renew Sustain Energy Rev*. 2020;133:110263. doi:10.1016/j.rser.2020.110263
11. Hossain MM, Gu M. Radiative Cooling: Principles, Progress, and Potentials. *Adv Sci*. 2016;3(7):1500360. doi:10.1002/advs.201500360
12. Kecebas MA, Menguc MP, Kosar A, Sendur K. Passive Radiative Cooling Design with Broadband Optical Thin-Film Filters. *J Quant Spectrosc Radiative Trans*. 2017;198:179-186. doi:10.1016/j.jqsrt.2017.03.046
13. Li W, Shi Y, Chen K, Zhu L, Fan S. A Comprehensive Photonic Approach for Solar Cell Cooling. *ACS Photon*. 2017;4(4):774-782. doi:10.1021/acsphotonics.7b00089
14. Hossain MM, Jia B, Gu M. A Metamaterial Emitter for Highly Efficient Radiative Cooling. *Adv Opt Mater*. 2015;3(8):1047-1051. doi:10.1002/adom.201500119
15. Perrakis G, Tasolamprou AC, Kenanakis G, Economou EN, Tzortzakis S, Kafesaki M. Combined Nano and micro structuring for enhanced radiative cooling and efficiency of photovoltaic cells. *Scientif. Rep*. 2021;11(1):11552. doi:10.1038/s41598-021-91061-1
16. Mandal J, Fu Y, Overvig AC, et al. Hierarchically Porous Polymer Coatings for Highly Efficient Passive Daytime Radiative Cooling. *Science*. 2018;362(6412):315-319. doi:10.1126/science.aat9513
17. Wang T, Wu Y, Shi L, Hu X, Chen M, Wu L. A Structural Polymer for Highly Efficient All-Day Passive Radiative Cooling. *Nature Commun*. 2021;12(1):365. doi:10.1038/s41467-020-20646-7
18. EuChemS. The 90 Natural Elements That Make Up Everythings: How Much Is There? Is That Enough? Is It Sustainable? Dataset, EUChemS; 2021.
19. Cagnoni M, Tibaldi A, Testa P, Dolado JS, Cappelluti F. Passive Radiative Cooling of Solar Cells by Low-Cost and Scalable Metamaterials: Physical Simulation and Efficiency Limits; 2022:1199606. doi:10.1117/12.2607489
20. Taylor HFW. *Cement Chemistry*. Second: Telford; 2004.
21. Dolado JS, Goracci G, Arrese-Igor S, et al. Radiative Cooling Properties of Portlandite and Tobermorite: Two Cementitious Minerals of Great Relevance in Concrete Science and Technology. *ACS Appl Opt Mater*. 2023. doi:10.1021/acsaom.3c00082
22. Lu G, She W, Tong X, Zuo W, Zhang Y. Radiative Cooling Potential of Cementitious Composites: Physical and Chemical Origins. *Cement Concr Composites*. 2021;119:104004. doi:10.1016/j.cemconcomp.2021.104004
23. Safi TS, Munday JN. Improving Photovoltaic Performance Through Radiative Cooling in Both Terrestrial and Extraterrestrial Environments. *Optics Express*. 2015;23(19):A1120. doi:10.1364/OE.23.0A1120
24. Shockley W, Queisser HJ. Detailed Balance Limit of Efficiency of *p-n* Junction Solar Cells. *J Appl Phys*. 1961;32(3):510-519. doi:10.1063/1.1736034
25. Luque López A, Hegedus S, eds. *Handbook of Photovoltaic Science and Engineering*. Second: Wiley; 2011.
26. Perrakis G, Tasolamprou AC, Kenanakis G, Economou EN, Tzortzakis S, Kafesaki M. Passive radiative cooling and other photonic approaches for the temperature control of photovoltaics: A comparative study for crystalline silicon-based architectures. *Optics Express*. 2020;28(13):18548. doi:10.1364/OE.388208
27. Çengel YA, Ghajar AJ. *Heat and Mass Transfer: Fundamentals & Applications*. Fifth: McGraw-Hill; 2015.
28. Bohnet M, Ullmann F, eds. *Ullmann's Encyclopedia of Industrial Chemistry*: Wiley; 2003.
29. Swartz ET, Pohl RO. Thermal Resistance at Interfaces. *Appl Phys Lett*. 1987;51(26):2200-2202. doi:10.1063/1.98939
30. Lai C-M, Hokoi S. Solar Façades: A Review. *Build Environ*. 2015;91:152-165. doi:10.1016/j.buildenv.2015.01.007
31. Águas H, Ram SK, Araújo A, et al. Silicon Thin Film Solar Cells on Commercial Tiles. *Energy Environ Sci*. 2011;4(11):4620. doi:10.1039/c1ee02303a
32. Hosseini T, Flores-Vivian I, Sobolev K, Kouklin N. Concrete Embedded Dye-Synthesized Photovoltaic Solar Cell. *Scientif Rep*. 2013;3(1):2727. doi:10.1038/srep02727
33. Iencinella D, Centurioni E, Grazia Busana M. Thin-Film Solar Cells on Commercial Ceramic Tiles. *Solar Energy Mater Solar Cells*. 2009;93(2):206-210. doi:10.1016/j.solmat.2008.09.030

34. Guerrero-Lemus R, Vega R, Kim T, Kimm A, Shephard LE. Bifacial Solar Photovoltaics - A Technology Review. *Renew Sustain Energy Rev*. 2016;60:1533-1549. doi:10.1016/j.rser.2016.03.041
35. Boriskina SV. An Ode to Polyethylene. *MRS Energy Sustainab*. 2019; 6(1):14. doi:10.1557/mre.2019.15
36. Ahmed S, Li S, Li Z, Xiao G, Ma T. Enhanced radiative cooling of solar cells by integration with heat pipe. *Appl Energy*. 2022;308:118363. doi:10.1016/j.apenergy.2021.118363
37. Tiedje T, Yablonovitch E, Cody GD, Brooks BG. Limiting Efficiency of Silicon Solar Cells. *IEEE Trans Electron Devices*. 1984;31(5):711-716. doi:10.1109/T-ED.1984.21594
38. Kirchartz T, Rau U. What Makes a Good Solar Cell? *Adv Energy Mater*. 2018;8(28):1703385. doi:10.1002/aenm.201703385
39. ASTM. Reference Air Mass 1.5 Spectra. Dataset ASTM G-173-03, NREL.
40. Würfel P. The Chemical Potential of Radiation. *J Phys C: Solid State Phys*. 1982;15(18):3967-3985. doi:10.1088/0022-3719/15/18/012
41. Levinshtein ME, Rumyantsev S, Shur M. *Handbook Series on Semiconductor Parameters. Vol. 1: Si, Ge, C (Diamond), GaAs, GaP, GaSb, InAs, InP, InSb*, Vol. 1: World scientific; 1996.
42. Schenk A. A Model for the Field and Temperature Dependence of Shockley-Read-Hall Lifetimes in Silicon. *Solid-State Electron*. 1992; 35(11):1585-1596. doi:10.1016/0038-1101(92)90184-E
43. Fell A, McIntosh KR, Altermatt PP, et al. Input Parameters for the Simulation of Silicon Solar Cells in 2014. *IEEE J Photovolt*. 2015;5(4): 1250-1263. doi:10.1109/JPHOTOV.2015.2430016
44. Huldt L, Nilsson NG, Svantesson KG. The Temperature Dependence of Band-to-Band Auger Recombination in Silicon. *Appl Phys Lett*. 2008;35(10):776-777. doi:10.1063/1.90974
45. Svantesson KG, Nilsson NG. The Temperature Dependence of the Auger Recombination Coefficient of Undoped Silicon. *J Phys C: Solid State Phys*. 1979;12(23):5111. doi:10.1088/0022-3719/12/23/019
46. Lin Y, Schlenker E, Zhou Z, Bermel P. RadCool: A Web-Enabled Simulation Tool for Radiative Cooling. In: Summer Undergraduate Research Fellowship (SURF) Symposium. Purdue University; 2017:42.
47. Berk A, Anderson GP, Acharya PK, et al. MODTRAN5: 2006 Update; 2006:62331F. doi:10.1117/12.665077
48. Gruginskie N, Cappelluti F, Bauhuis GJ, et al. Electron Radiation-Induced Degradation of GaAs Solar Cells with Different Architectures. *Progr Photovolt: Res Appl*. 2020;28(4):266-278.
49. McEvoy AJ, Markvart T, Castañer L, eds. *Practical Handbook of Photovoltaics: Fundamentals and Applications*. Second: Academic Press; 2012.
50. Liou JJ, Wong WW. Comparison and Optimization of the Performance of Si and GaAs Solar Cells. *Solar Energy Materials and Solar Cells*. 1992;28(1):9-28.
51. Kasap S, Capper P, eds. *Springer Handbook of Electronic and Photonic Materials*: Springer; 2006.
52. Xian Y, Zhang P, Zhai S, Yuan P, Yang D. Experimental Characterization Methods for Thermal Contact Resistance: A Review. *Appl Thermal Eng*. 2018;130:1530-1548. doi:10.1016/j.applthermaleng.2017.10.163

How to cite this article: Cagnoni M, Testa P, Dolado JS, Cappelluti F. Extended detailed balance modeling toward solar cells with cement-based radiative coolers. *Prog Photovolt Res Appl*. 2023;1-10. doi:10.1002/pip.3758